



**HAL**  
open science

# Matter Wave Transport and Anderson Localization in Anisotropic 3D Disorder

Marie Piraud, Luca Pezzé, Laurent Sanchez-Palencia

► **To cite this version:**

Marie Piraud, Luca Pezzé, Laurent Sanchez-Palencia. Matter Wave Transport and Anderson Localization in Anisotropic 3D Disorder. 2011. hal-00651193v1

**HAL Id: hal-00651193**

**<https://hal-iogs.archives-ouvertes.fr/hal-00651193v1>**

Preprint submitted on 13 Dec 2011 (v1), last revised 13 Sep 2012 (v3)

**HAL** is a multi-disciplinary open access archive for the deposit and dissemination of scientific research documents, whether they are published or not. The documents may come from teaching and research institutions in France or abroad, or from public or private research centers.

L'archive ouverte pluridisciplinaire **HAL**, est destinée au dépôt et à la diffusion de documents scientifiques de niveau recherche, publiés ou non, émanant des établissements d'enseignement et de recherche français ou étrangers, des laboratoires publics ou privés.

# Matter Wave Transport and Anderson Localization in Anisotropic 3D Disorder

M. Piraud, L. Pezzé,<sup>\*</sup> and L. Sanchez-Palencia

*Laboratoire Charles Fabry, Institut d'Optique, CNRS, Univ Paris Sud,*

*2 avenue Augustin Fresnel, F-91127 Palaiseau cedex, France*

(Dated: December 13, 2011)

## Abstract

We study quantum transport in anisotropic 3D disorder and show that non rotation invariant correlations can induce rich diffusion and localization properties. For instance, structured finite-range correlations can lead to the inversion of the transport anisotropy. Moreover, working beyond the self-consistent theory of localization, we include the disorder-induced shift of the energy states and show that it strongly affects the mobility edge. Implications to recent experiments are discussed.

PACS numbers: 03.75.-b, 05.60.Gg, 67.85.-d, 72.15.Rn

Coherent transport in disordered media is strongly affected by anisotropy effects. This occurs in a variety of systems, e.g. electrons in MOSFETs [1], diffusion-wave spectroscopy [2], biomedical imaging [3], and light in liquid crystals [4], phosphides [5], or microcavities [6]. So far, theoretical studies mainly focused on models of disorder made with isotropic impurities in anisotropic media [7, 8] or stretched scatterers in isotropic media [9], which fairly describe the above systems. However, much less is known about coherent transport in disorders with more complex anisotropic correlations.

Here we study disorders with structured, anisotropic, finite-range correlations and show that they can lead to rich diffusion and localization properties. This issue is particularly relevant to optical disorder, which correlations can be controlled [10], and we focus on the two configurations recently used to study Anderson localization (AL) of matter waves [11, 12]. Using the approach of Ref. [7], we quantitatively determine the incoherent diffusion, quantum-corrected diffusion and localization tensors versus the particle energy. A striking result is that weak structured correlations can induce strong anisotropy effects, for instance the inversion of the transport anisotropy. In addition, we extend the approach of Ref. [7] by including the disorder-induced shift of the energy states. We show that it strongly affects the mobility edge and discuss implications to the very challenging experimental determination of the mobility edge.

*Quantum transport.* — The building block to describe wave propagation in random media is the four-point vertex  $\Phi$ . It is explicitly written  $\Phi_{\mathbf{k},\mathbf{k}'}(\mathbf{q}, \omega, E) \equiv \overline{\langle \mathbf{k}_+ | G(E_+) | \mathbf{k}'_+ \rangle \langle \mathbf{k}'_- | G^\dagger(E_-) | \mathbf{k}_- \rangle}$  in momentum space, with  $G$  the retarded Green operator,  $\mathbf{k}_\pm \equiv \mathbf{k} \pm \mathbf{q}/2$  and  $\mathbf{k}'_\pm \equiv \mathbf{k}' \pm \mathbf{q}/2$  the left and right entries,  $E_\pm \equiv E \pm \hbar\omega/2$ , and  $(\mathbf{q}, \omega)$  the Fourier conjugates of the space and time variables [13]. Without any approximation,  $\Phi$  is governed by the Bethe-Salpeter equation (BSE) [14]

$$\Phi = \overline{G} \otimes \overline{G}^\dagger + \overline{G} \otimes \overline{G}^\dagger U \Phi \quad (1)$$

where  $U$  is the vertex function including all irreducible scattering diagrams. The first term in Eq. (1) describes uncorrelated propagation of the field and its conjugate in the disordered medium. The second term accounts for all correlations in the density propagation. In the independent scattering (Boltzmann) and weak disorder (Born) approximations [7],  $U_{\mathbf{k},\mathbf{k}'}(\mathbf{q}, \omega, E) \simeq \tilde{C}(\mathbf{k} - \mathbf{k}')$ , where  $\tilde{C}(\mathbf{k})$  is the disorder power spectrum (Fourier transform of the correlation function [13]) and the disorder is defined with zero mean value. At this stage, only the ladder diagrams in Eq. (1) are retained. It represents an infinite series of indepen-

dent scattering events, which leads to Drude-like diffusion. The solution of the BSE (1) is then dominated in the long time ( $\omega \rightarrow 0$ ) and large distance ( $\mathbf{q} \rightarrow 0$ ) limit by a diffusion pole [14], which reads

$$\Phi_{\mathbf{k},\mathbf{k}'}(\mathbf{q}, \omega, E) = \frac{2\pi}{\hbar N_0(E)} \frac{\delta(E - \epsilon(\mathbf{k})) \delta(E - \epsilon(\mathbf{k}'))}{-i\omega + \mathbf{q} \cdot \mathbf{D}_B(E) \cdot \mathbf{q}} \quad (2)$$

in the on-shell approximation [such that  $\epsilon(\mathbf{k}) = \epsilon(\mathbf{k}') = E$ , where  $\epsilon(\mathbf{k})$  is the disorder-free dispersion relation] and with  $N_0(E)$  the disorder-free density of states. The components of the Boltzmann diffusion tensor  $\mathbf{D}_B(E)$  are [7]

$$D_B^{i,j}(E) = \frac{1}{N_0(E)} \left\{ \left\langle \tau_{E,\hat{\mathbf{k}}} v_i v_j \right\rangle_{\hat{\mathbf{k}}|E} \right. \\ \left. + \frac{2\pi}{\hbar} \sum_{\lambda_E^n \neq 1} \frac{\lambda_E^n}{1 - \lambda_E^n} \left\langle \tau_{E,\hat{\mathbf{k}}} v_i \phi_{E,\hat{\mathbf{k}}}^n \right\rangle_{\hat{\mathbf{k}}|E} \left\langle \tau_{E,\hat{\mathbf{k}}} v_j \phi_{E,\hat{\mathbf{k}}}^n \right\rangle_{\hat{\mathbf{k}}|E} \right\}, \quad (3)$$

where  $v_i = \hat{\mathbf{u}}_i \cdot \nabla_{\mathbf{k}} \epsilon(\mathbf{k}) / \hbar$  is the velocity along axis  $i$ ,  $\tau_{E,\hat{\mathbf{k}}} = \hbar / 2\pi \langle \tilde{C}(k_{E,\hat{\mathbf{k}}} \hat{\mathbf{k}} - \mathbf{k}') \rangle_{\hat{\mathbf{k}}'|E}$  [with  $\hat{\mathbf{k}} \equiv \mathbf{k}/|\mathbf{k}|$  and  $k_{E,\hat{\mathbf{k}}}$  defined by  $\epsilon(k_{E,\hat{\mathbf{k}}} \hat{\mathbf{k}}) = E$ ] is the on-shell scattering mean free time, and  $\langle \dots \rangle_{\hat{\mathbf{k}}|E} \equiv \int \frac{d^d \mathbf{k}}{(2\pi)^d} \dots \delta[E - \epsilon(\mathbf{k})]$  represents integration over the  $\mathbf{k}$ -space shell defined by  $\epsilon(\mathbf{k}) = E$ . The functions  $\phi_{E,\hat{\mathbf{k}}}^n$  and the real-valued positive numbers  $\lambda_E^n$  are the solutions of the integral eigenproblem

$$\frac{2\pi}{\hbar} \left\langle \tau_{E,\hat{\mathbf{k}}} \tilde{C}(k_{E,\hat{\mathbf{k}}} \hat{\mathbf{k}} - \mathbf{k}') \phi_{E,\hat{\mathbf{k}}}^n \right\rangle_{\hat{\mathbf{k}}'|E} = \lambda_E^n \phi_{E,\hat{\mathbf{k}}}^n, \quad (4)$$

normalized by  $\frac{2\pi}{\hbar} \langle \tau_{E,\hat{\mathbf{k}}} \phi_{E,\hat{\mathbf{k}}}^n \phi_{E,\hat{\mathbf{k}}}^m \rangle_{\hat{\mathbf{k}}|E} = \delta_{n,m}$  [7]. In the following, we numerically solve the above equations and determine  $\mathbf{D}_B(E)$  for anisotropic 3D models of disorder.

*Anisotropic diffusion in 3D speckles.* — Let us consider ultracold matter waves in speckle potentials [10]. The underlying medium is the (isotropic) vacuum, for which  $\epsilon(\mathbf{k}) = \hbar^2 \mathbf{k}^2 / 2m$ . In Ref. [11] (*single-speckle* configuration), an optical disorder is obtained using a single Gaussian laser beam of waist  $w$  and wavelength  $\lambda_L$ , propagating along the  $z$  axis, passed through a ground-glass plate and focused by an optical lens of focal distance  $f$ . The disorder correlation function  $C(\mathbf{r})$  has correlation lengths  $\sigma_{\parallel} = 4\lambda_L f^2 / \pi w^2$  in the propagation axis ( $z$ ) and  $\sigma_{\perp} = \lambda_L f / \pi w$  in the orthogonal plane ( $x, y$ ) [15]. In general  $4f > w$ , and  $C(\mathbf{r})$  is elongated along  $z$  ( $\sigma_{\parallel} / \sigma_{\perp} \simeq 5.8$  in Refs. [11, 12]). The corresponding disorder power spectrum  $\tilde{C}(\mathbf{k})$  is isotropic in the  $(k_x, k_y)$  plane but significantly shorter in the  $k_z$  axis [see Fig. 1(a)]. In Ref. [12] (*coherent-speckles* configuration), the disorder results from the interference of two mutually coherent and orthogonal speckle fields, propagating along the  $z$

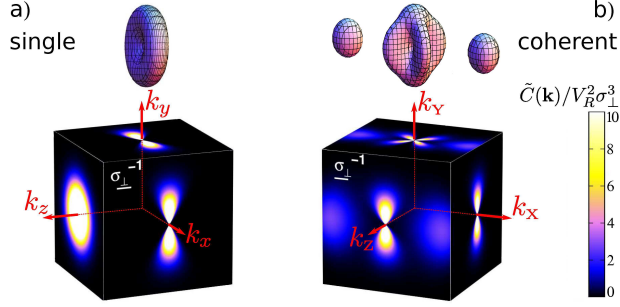


Figure 1. (color online) Disorder power spectrum  $\tilde{C}(\mathbf{k})$  for the (a) single-speckle and (b) coherent-speckles cases (Fourier transforms of the formulas in note [15]) with the parameters of Refs. [11, 12] (see text). The functions  $\tilde{C}(\mathbf{k})$  are represented as iso-value surfaces (at  $2V_R^2\sigma_\perp^3$ ) and cuts in the planes defined by the transport eigenaxes (see text):  $\{\hat{\mathbf{u}}_x, \hat{\mathbf{u}}_y, \hat{\mathbf{u}}_z\}$  for (a) and  $\{\hat{\mathbf{u}}_X \equiv (\hat{\mathbf{u}}_x - \hat{\mathbf{u}}_z)/\sqrt{2}, \hat{\mathbf{u}}_Y \equiv \hat{\mathbf{u}}_y, \hat{\mathbf{u}}_Z \equiv (\hat{\mathbf{u}}_x + \hat{\mathbf{u}}_z)/\sqrt{2}\}$  for (b).

and  $x$  axes, respectively. The power spectrum  $\tilde{C}(\mathbf{k})$  then shows a complex structure, made of the sum of two orthogonally-oriented spectra, similar to that of the single-speckle case, plus a coherence term [15]. The latter mainly creates two broad structures (*bumps*), centered on the  $\hat{\mathbf{k}}_X \equiv (\hat{\mathbf{k}}_x - \hat{\mathbf{k}}_z)/\sqrt{2}$  axis [see Fig. 1(b)], at  $k_X \simeq \pm 3.8\sigma_\perp^{-1}$  for  $\lambda_L/\sigma_\perp \simeq 2.16$  (as in Ref. [12]). In the following we call  $V_R \equiv \sqrt{\tilde{C}(\mathbf{r} = 0)}$  the amplitude and  $E_{\sigma_\perp} \equiv \hbar^2/m\sigma_\perp^2$  the correlation energy of the disorder.

We now discuss the behavior of the components of  $\mathbf{D}_B(E)$ , shown in Fig. 2 for the two above configurations. The transport eigenaxes follow from the symmetries of  $\tilde{C}(\mathbf{k})$ . For the single-speckle case [Fig. 2(a)], all quantities are isotropic in the  $(x, y)$  plane. We find that the scattering time is shorter along  $z$  ( $\tau_{\hat{\mathbf{k}}_z, E} < \tau_{\hat{\mathbf{k}}_{\{x, y\}}, E}$ ). It is due to the wider extension of  $\tilde{C}(\mathbf{k})$  in the plane  $(x, y)$  orthogonal to  $z$ , which offers more scattering channels to particles travelling along  $z$ . We however find that the orbitals  $\phi_{E, \hat{\mathbf{k}}}^n$  contributing to  $D_B^z$  in Eq. (4) are associated to larger values of  $\lambda_E^n$ , and the anisotropy of  $\mathbf{D}_B$  is inversed with respect to that of  $\tau_{\hat{\mathbf{k}}, E}$  ( $D_B^z > D_B^{x, y}$ ).

In order to get further insight, it is useful to note that, for isotropic systems (see also Refs. [16, 17]), Eq. (4) is solved by the spherical harmonics  $Y_l^m$ , and that only the first term plus the  $Y_1^m$  ( $p$ -level) harmonics contribute to  $\mathbf{D}_B$  in Eq. (3). For our anisotropic disorder, we find that the calculated orbitals  $\phi_{E, \hat{\mathbf{k}}}^n$  are topologically similar to the spherical harmonics, i.e. they show similar nodal surfaces. We thus refer to " $Y_l^m$ -like" orbitals. Note that here

the  $\lambda_E^n$  are not degenerated in a given  $l$ -like level.

Within the on-shell Born approach, a particle of energy  $E$  probes  $\tilde{C}(\mathbf{k})$  inside the  $\mathbf{k}$ -space sphere of radius  $2k_E$  ( $k_E \equiv \sqrt{2mE}/\hbar$ ). For  $2k_E \ll \sigma_\perp^{-1}$ ,  $\tilde{C}(\mathbf{k})$  shows a strong anisotropic divergence due to long-range correlations, which suppress the white-noise limit. We have  $\tilde{C}(\mathbf{k}) \sim \tilde{c}(\hat{\mathbf{k}})/|\mathbf{k}|$  with  $\tilde{c}(\hat{\mathbf{k}}) = \exp[-(\sigma_\parallel/2\sigma_\perp)^2 \hat{k}_z^2 / (\hat{k}_x^2 + \hat{k}_y^2)] / (\hat{k}_x^2 + \hat{k}_y^2)^{1/2}$ . This scaling shows that  $\tau_{\hat{\mathbf{k}},E}$  and  $\lambda_E^n$  do not depend on  $E$ , and  $\phi_{E,\hat{\mathbf{k}}}^n$  is of the form  $\varphi^n(\hat{\mathbf{k}})/\sqrt{k_E}$ . All terms in Eq. (3) are topologically unchanged and scale as  $E$ . Then, the anisotropy of  $\mathbf{D}_B$  remains unchanged down to arbitrary low  $E$  and  $D_B^u \propto E$ , as observed in Fig. 2. More precisely, we find that  $D_B^{x,y}$  is dominated by the first term in Eq. (3) and  $D_B^z$  by the  $Y_1^0$ -like orbital. For  $2k_E \gg \sigma_\perp^{-1}$ , the situation changes: we find that, while  $D_B^z$  is still dominated by the  $Y_1^0$ -like orbital,  $D_B^{x,y}$  is now dominated by the  $Y_1^{\pm 1}$ -like orbitals with a contribution of the  $Y_3^{\pm 1}$ -like orbitals increasing with  $E$ . In this regime, we find  $\tau_{\hat{\mathbf{k}},E} \propto k_E$  and  $\phi_{E,\hat{\mathbf{k}}}^n \propto 1/k_E$ . Then, assuming weak topological change of the orbitals and the scaling  $1 - \lambda_E^n \propto 1/E$  (found numerically), we get  $D_B^u(E) \propto E^{5/2}$ , as observed in Fig. 2. This scaling was also found in other isotropic models of disorder [16]. Remarkably, in spite of the different contributing terms in Eq. (3) at low and high  $E$ , the transport anisotropy is nearly independent of  $E$ , with  $D_B^z/D_B^{x,y} \simeq 10$  [see inset of Fig. 2(a)].

For the coherent-speckles case [Fig. 2(b)], we find similar general trends. However, due to the crossing of the two speckles, the transport eigenaxes are now the bisectors  $\{\hat{\mathbf{X}}, \hat{\mathbf{Z}}\} = (\hat{\mathbf{x}} \mp \hat{\mathbf{z}})/\sqrt{2}$  and  $\hat{\mathbf{Y}} = \hat{\mathbf{y}}$ , and the anisotropy is much smaller. The function  $\tilde{C}(\mathbf{k})$  shows no rotation invariance and, strictly,  $D_B^X$ ,  $D_B^Y$  and  $D_B^Z$  are all different. For  $2k_E \ll 3.8\sigma_\perp^{-1}$ , the behavior of  $\mathbf{D}_B(E)$  is governed by the central structure of  $\tilde{C}(\mathbf{k})$ , which is marginally affected by the coherence of the two crossed speckles [15]. The directions  $\hat{\mathbf{X}}$  and  $\hat{\mathbf{Z}}$  are then nearly identical but the direction  $\hat{\mathbf{Y}}$  is different: we find  $D_B^Y < D_B^X \simeq D_B^Z$  with  $D_B^{X,Z}/D_B^Y \simeq 1.8$ . For  $2k_E \gtrsim 3.8\sigma_\perp^{-1}$ , the presence of the bumps of  $\tilde{C}(\mathbf{k})$  at  $\mathbf{k} \simeq \pm 3.8\sigma_\perp^{-1}\hat{\mathbf{k}}_X$  [see Fig. 1(b)] makes the situation particularly interesting by strongly affecting the scattering of particles along  $\hat{\mathbf{X}}$ . The scattering time  $\tau_{E,\hat{\mathbf{k}}}$  becomes highly anisotropic and the orbital dominating  $D_B^X$  is strongly distorted. Then,  $D_B^X$  is reduced and the corresponding anisotropy factor drops by a factor of  $\simeq 4$ . This effect is strong enough to invert the transport anisotropy, so that  $D_B^X < D_B^Y < D_B^Z$  [18].

*Localization.*— We now consider quantum interference corrections to Boltzmann diffusion by including the maximally-crossed diagrams (Cooperon and Hikami contributions) into the

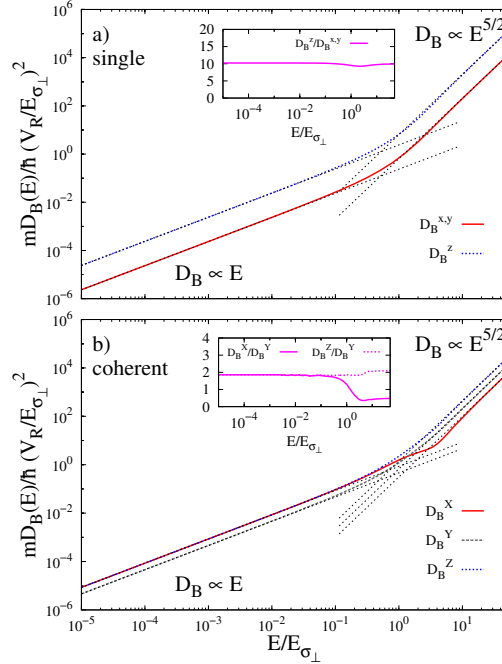


Figure 2. (color online) Eigencomponents of the Boltzmann diffusion tensor (diffusion coefficients) along the transport eigenaxes (see caption of Fig. 1) for the (a) single and (b) coherent speckle configurations. The dotted lines are power-law fits ( $D_B^u \propto E^{\gamma_u}$ ) to the data in the low and high energy limits. The insets show the transport anisotropy factors.

vertex  $U$ . It yields the dynamic diffusion tensor  $\mathbf{D}_*(\omega, E) = \mathbf{D}_B(E) + \Delta\mathbf{D}(\omega, E)$  with [7]

$$\Delta\mathbf{D}(\omega, E) = \frac{-\mathbf{D}_B(E)}{\pi\hbar N_0(E)} \int \frac{d\mathbf{q}}{(2\pi)^d} \frac{1}{-i\omega + \mathbf{q} \cdot \mathbf{D}_B(E) \cdot \mathbf{q}}. \quad (5)$$

Following the standard self-consistent theory [19], the above equations are solved for  $\mathbf{D}_*(\omega, E)$  after replacing  $\mathbf{D}_B(E)$  by  $\mathbf{D}_*(\omega, E)$  in the integrand of Eq. (5). Since the diffusive dynamics is relevant only on length scales larger than the Boltzmann mean free path,  $l_B^u(E) \equiv d\sqrt{m/2E}D_B^u(E)$  along each transport eigenaxis, we regularize the ultraviolet divergence of the integral in Eq. (5) by setting an elliptic cut-off of radii  $1/l_B^u$ . Proceeding (in 3D) in the long time limit ( $\omega \rightarrow 0$ ), a threshold energy  $E_c$  appears, solution of  $D_B^{\text{av}}(E_c) \equiv \det\{\mathbf{D}_B(E_c)\}^{1/3} = \hbar/\sqrt{3\pi}m$ . For  $E > E_c$ ,  $\mathbf{D}_*(\omega, E)$  converges to a real definite positive tensor when  $\omega \rightarrow 0$ . It describes anisotropic normal diffusion, characterized by the propagation kernel (2) where  $\mathbf{D}_B(E)$  is substituted to the quantum-corrected diffusion tensor  $\mathbf{D}_*(E) \equiv \lim_{\omega \rightarrow 0} \mathbf{D}_*(\omega, E)$ . For  $E < E_c$ , one finds  $\mathbf{D}_*(\omega, E) \sim -i\omega\mathbf{\Lambda}(E)$  for  $\omega \rightarrow 0$ , where  $\mathbf{\Lambda}(E)$  is a real positive definite tensor. It characterizes exponential localization in the

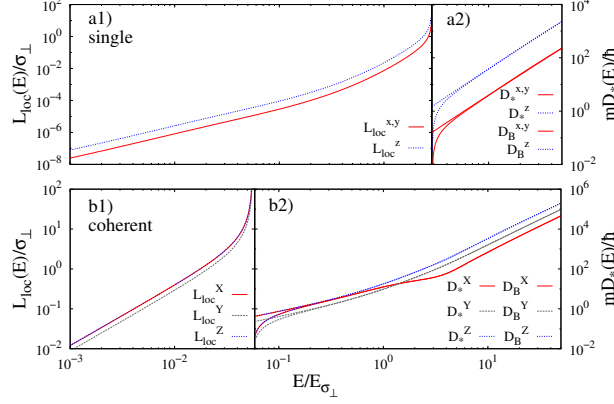


Figure 3. (color online) Eigencomponents of the localization (left column;  $E < E_c$ ) and quantum-corrected diffusion (right column;  $E > E_c$ ) tensors for the single (upper row;  $V_R = 7.1E_{\sigma_{\perp}}$ ) and coherent (lower row;  $V_R = 0.35E_{\sigma_{\perp}}$ ) speckle configurations. The Boltzmann diffusion coefficients are plotted for comparison (thin lines on the right column).

propagation kernel (2), with the anisotropic localization tensor  $\mathbf{L}_{\text{loc}}(E) \equiv \sqrt{\Lambda(E)}$ .

Figure 3 shows the components of  $\mathbf{L}_{\text{loc}}$  (for  $E < E_c$ ) and  $\mathbf{D}_*$  (for  $E > E_c$ ) for the single-speckle and coherent-speckles cases (with the parameters of Refs [11, 12]). We observe that the anisotropy factors of  $\mathbf{L}_{\text{loc}}$  and  $\mathbf{D}_*$  are nearly independent of  $E$ , except for the inversion of anisotropy of the coherent-speckles case [20]. In fact, the behavior of  $\mathbf{L}_{\text{loc}}$  and  $\mathbf{D}_*$  is completely determined by that of  $\mathbf{D}_B$  (see above). This is due to a remarkable property of Eq. (5), showing that the quantum corrections  $\Delta\mathbf{D}(\omega, E)$  do not explicitly depend on the disorder [i.e. on  $\tilde{C}(\mathbf{k})$ ], but only on  $\mathbf{D}_B(E)$  [7]. For instance,  $\mathbf{D}_*(\omega, E)$  has the same eigenaxes and anisotropy factors as  $\mathbf{D}_B(E)$ . For  $E < E_c$ , the anisotropy factors of  $\mathbf{L}_{\text{loc}}(E)$  are thus the square roots of those of  $\mathbf{D}_B(E)$ . In the low  $E$  limit, we find  $L_{\text{loc}}^u(E) \propto (D_B^u/D_B^{\text{av}})^{1/2} E^{3/2}$ . When  $E$  increases,  $L_{\text{loc}}^u(E)$  grows and finally diverges at  $E_c$ . For  $E > E_c$ , the anisotropy factors of  $\mathbf{D}_*(E)$  are the same as those of  $\mathbf{D}_B(E)$ . The quantum corrections are significant only close to  $E_c$ . For higher values of  $E$ ,  $\mathbf{D}_*(E) \simeq \mathbf{D}_B(E)$ , and in the high  $E$  limit,  $D_*^u(E) \propto (D_B^u/D_B^{\text{av}})E^{5/2}$ .

*Mobility edge.*— So far, we have used the usual on-shell approach, which is expected to fairly describe quantum transport [7, 16, 19]. It however neglects the real part of the particle's self-energy in the disorder,  $\Sigma'(\mathbf{k}, E) \equiv \text{P} \int \frac{d\mathbf{k}'}{(2\pi)^d} \frac{\tilde{C}(\mathbf{k}-\mathbf{k}')}{E-\epsilon_{\mathbf{k}'}}$  (with P the Cauchy principal value), which may be a questionable approximation, in particular for estimating the mobility edge. We incorporate  $\Sigma'(\mathbf{k}, E)$  into the theory by averaging, in first approxi-

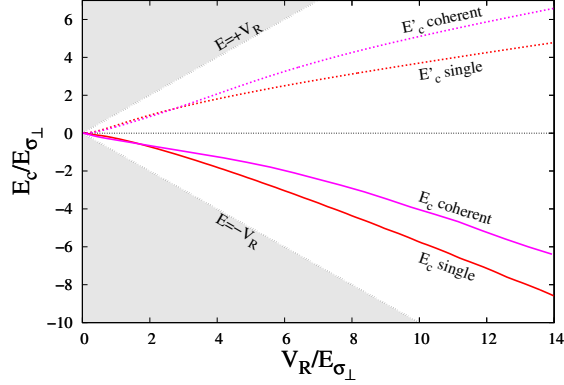


Figure 4. (color online) On-shell ( $E'_c$ ) and corrected ( $E_c$ ) mobility edges as functions of the disorder amplitude  $V_R$  for the single-speckle and coherent-speckles configurations.

mation, its  $\mathbf{k}$ -angle dependence [21]. It amounts to replace the on-shell prescription by  $\epsilon(\mathbf{k}) = E' \equiv E - \Delta(E)$  with

$$\Delta(E) \equiv \frac{1}{4\pi} \int_{\epsilon(\mathbf{k})=E-\Delta(E)} d\Omega_{\hat{\mathbf{k}}} \Sigma'(\mathbf{k}, E) \quad (6)$$

where  $\Omega_{\hat{\mathbf{k}}}$  is the  $\mathbf{k}$ -space solid angle. Within this approach, all preceding quantities are now regarded as functions of  $E'$  instead of  $E$ . In particular, the mobility edge  $E_c$  is the solution of  $E_c - \Delta(E_c) = E'_c$ , where  $E'_c$  is determined using the on-shell approach (see above). The on-shell ( $E'_c$ ) and corrected ( $E_c$ ) mobility edges are shown in Fig. 4. It is eye-catching that the shift of the energy states completely changes the behavior of the mobility edge. While  $E'_c$  is positive and increases with  $V_R$ , we find that  $E_c$  is negative and decreases with  $V_R$ . For  $V_R \lesssim E_{\sigma_{\perp}}$ , we find a similar behavior of  $E_c$  as that obtained using the SCBA method for isotropic disorders [17]. For larger values of  $V_R$ ,  $E_c$  further decreases consistently with the idea that it should approach the percolation threshold deep in the regime of classical disorder ( $V_R \gg E_{\sigma_{\perp}}$ ) [22].

*Discussion.*— Focusing on two models of optical disorder, we have shown that long-range correlations that break rotation invariance can lead to a non-trivial energy dependence of the transport and localization tensors. In the single-speckle case [11], the transport anisotropy is surprisingly constant ( $D_*^z/D_*^{x,y} \simeq 10$  in the diffusion regime and  $L_{\text{loc}}^z/L_{\text{loc}}^{x,y} \simeq 3.2$  in the localization regime). This holds down to arbitrary small energy, due to anisotropic long-range correlations, which suppress the white-noise limit. In the coherent-speckles case [12], we found similar properties at low energy (with  $D_*^X/D_*^Y \simeq D_*^Z/D_*^Y \simeq 1.8$  and

$L_{\text{loc}}^X/L_{\text{loc}}^Y \simeq L_{\text{loc}}^Z/L_{\text{loc}}^Y \simeq 1.3$ ). Most interestingly, the two structures of the power spectrum centered at  $k_X \simeq \pm 3.8\sigma_{\perp}^{-1}$  strongly enhance the scattering along  $\hat{X}$  of particles with energy such that  $2k_E \gtrsim 3.8\sigma_{\perp}^{-1}$ . As a result,  $D_{\text{B}}^X$  drops below  $D_{\text{B}}^Y$  and  $D_{\text{B}}^Z$ , thus inverting the transport anisotropy. Our results provide a guideline to future studies of anisotropy effects in experiments with ultracold atoms in 3D disorder [23]. They may also be extended to 2D configurations [24].

Moreover, we have calculated the 3D mobility edge by extending the standard on-shell approach, including the real part of the self-energy. Let us discuss our predictions in view of what has been experimentally achieved so far. Comparing to Ref. [11], our calculations significantly differ in amplitude and sign from experimental values (e.g. for  $V_{\text{R}} = 600 \text{ nK} \times k_{\text{B}} \simeq 7.1E_{\sigma_{\perp}}$ , we find  $E_c \simeq -300 \text{ nK} \times k_{\text{B}}$ , while  $+900 \text{ nK} \times k_{\text{B}}$  is measured). However, the method used in Ref. [11] to infer  $E_c$  from the localized fraction neglects the distortion of the energy distribution induced by the disorder. This method is questionable because the latter is, in particular, a necessary ingredient to account for negative energy states (i.e. below the disorder mean value). Comparing to Ref. [12], we find that  $\Delta(E_c)$  as calculated here is of the same order of magnitude as the heuristic shift introduced in Ref. [12] (e.g. for  $V_{\text{R}} = h \times 680 \text{ Hz} \simeq 0.35E_{\sigma_{\perp}}$ , we find  $\Delta(E_c)/h = -390 \text{ Hz}$ , and the heuristic shift is  $-225 \text{ Hz}$ ). This signals that  $\Sigma'$  provides a significant contribution to this heuristic shift. A precise test of the present theory would however require a reliable determination of the energy distribution in ultracold-atom experiments, which is not available yet. Finally, we note that our approach may be improved by performing a fully off-shell calculation.

We thank B. DeMarco, F. Jendrzejewski, V. Josse, and B. van Tiggelen for useful discussions. This research was supported by ERC (contract No. 256294). The numerical calculations were performed on the LUMAT cluster (FR LUMAT 2764) with the assistance of M. Besbes.

---

\* Present address: INO-CNR and LENS, Firenze (Italy)

- [1] D. J. Bishop *et al.*, Phys. Rev. B **30**, 3539 (1984).
- [2] D. J. Pine *et al.*, Phys. Rev. Lett. **60**, 1134 (1988).
- [3] S. Nickell *et al.*, Phys. Med. Biol. **45**, 2873 (2000).

- [4] M. H. Kao *et al.*, Phys. Rev. Lett. **77**, 2233 (1996); D. S. Wiersma *et al.*, *ibid.* **83**, 4321 (1999).
- [5] P. M. Johnson *et al.*, Phys. Rev. Lett. **89**, 243901 (2002).
- [6] M. Gurioli *et al.*, Phys. Rev. Lett. **94**, 183901 (2005).
- [7] P. Wölfle and R. N. Bhatt, Phys. Rev. B **30**, 3542 (1984).
- [8] B. C. Kaas *et al.*, Phys. Rev. Lett. **100**, 123902 (2008).
- [9] B. A. van Tiggelen *et al.*, Phys. Rev. Lett. **77**, 639 (1996); H. Stark and T. C. Lubensky, Phys. Rev. E **55**, 514 (1997).
- [10] L. Sanchez-Palencia and M. Lewenstein, Nature Phys. **6**, 87 (2010); D. Clément *et al.*, New J. Phys. **8**, 165 (2006).
- [11] S. S. Kondov *et al.*, Science **334**, 66 (2011).
- [12] F. Jendrzejewski *et al.*, arXiv:1108.0137v1.
- [13] Here, we use  $\tilde{f}(\mathbf{q}, \omega) \equiv \int d\mathbf{r} dt f(\mathbf{r}, t) \exp[-i(\mathbf{q} \cdot \mathbf{r} - \omega t)]$ .
- [14] J. Rammer, *Quantum Transport Theory* (Perseus Books, Reading, Mass., 1998).
- [15] In the paraxial approximation, we find explicit formulas: For the single-speckle case,  $C(\mathbf{r}) = V_{\text{R}}^2 c_{\text{1sp}}^2(x, y, z)$  with
- $$c_{\text{1sp}}(x, y, z) = \frac{1}{\sqrt{1 + 4z^2/\sigma_{\parallel}^2}} \exp \left[ -\frac{(x^2 + y^2)/2\sigma_{\perp}^2}{1 + 4z^2/\sigma_{\parallel}^2} \right].$$
- For the coherent-speckles case,  $C(\mathbf{r}) = (V_{\text{R}}/2)^2 \times \{c_{\text{1sp}}^2(x, y, z) + c_{\text{1sp}}^2(z, y, x) + 2c_{\text{coh}}(x, y, z)\}$  with
- $$c_{\text{coh}}(\mathbf{r}) = c_{\text{1sp}}(x, y, z) \times c_{\text{1sp}}(z, y, x) \frac{(1 + 4\frac{xz}{\sigma_{\parallel}^2}) \cos[\phi(\mathbf{r})] + 2\frac{x-z}{\sigma_{\parallel}} \sin[\phi(\mathbf{r})]}{\sqrt{1 + 4z^2/\sigma_{\parallel}^2} \sqrt{1 + 4x^2/\sigma_{\parallel}^2}}$$
- and  $\phi(\mathbf{r}) = \frac{2\pi}{\lambda_{\text{L}}}(x - z) - \frac{z}{\sigma_{\perp}^2 \sigma_{\parallel}} \frac{x^2 + y^2}{1 + 4z^2/\sigma_{\parallel}^2} - \frac{x}{\sigma_{\perp}^2 \sigma_{\parallel}} \frac{z^2 + y^2}{1 + 4x^2/\sigma_{\parallel}^2}$ .
- [16] R. C. Kuhn *et al.*, New J. Phys. **9**, 161 (2007).
- [17] S. E. Skipetrov *et al.*, Phys. Rev. Lett. **100**, 165301 (2008); A. Yedjour and B. A. van Tiggelen, Eur. Phys. J. D **59**, 249 (2010).
- [18] For incoherent crossed speckles, we found  $D_{\text{B}}^X = D_{\text{B}}^Z \simeq 1.8D_{\text{B}}^Y$ , up to arbitrary large values of  $E$ .
- [19] D. Vollhardt and P. Wölfle, in *Electronic Phase Transitions*, Eds. W. Hanke and Y. Kopalev (Elsevier, Berlin, 1992).
- [20] In Fig. 3, the inversion occurs in the diffusion regime. For higher values of  $V_{\text{R}}$ , it can be in the

localization regime.

- [21] This approximation is justified *a posteriori* by the weak  $\mathbf{k}$ -angle variations of  $\Sigma'$  around its mean value at  $E_c$  (with standard deviations less than 10 – 15%).
- [22] B. I. Shklovskii, *Semicond.* **42**, 909 (2008).
- [23] In Ref. [12], the images are taken in the  $y - z$  plane. It only gives access to  $D^y = D^Y$  and  $D^z = (D^X + D^Z)/2$ , which do not show the inversion of the transport anisotropy.
- [24] M. Robert-de-Saint-Vincent *et al.*, *Phys. Rev. Lett.* **104**, 220602 (2010); L. Pezzé *et al.*, *New J. Phys.* **13**, 095015 (2011).